Iranian Journal of Oil & Gas Science and Technology, Vol. 9 (2020), No. 3, pp. 44–60
http://ijogst.put.ac.ir

Investigation into Mechanism of Hydrogen Induced Cracking Failure in Carbon Steel: A Case Study of Oil and Gas Industry

Mohsen Asadipoor[1,2], Ali Pourkamali Anaraki[3]*, Javad Kadkhodapour[4], Seyed Mohammad Hossein Sharifi[5], and Afrooz Barnoush[6]

[1] Ph.D. Candidate, Department of Mechanical Engineering, Shahid Rajaee Teacher Training University, Tehran, Iran
[2] Ph.D. Candidate, Department of Mechanical and Industrial Engineering, Norwegian University of Science and Technology, Trondheim, Norway
[3] Associate Professor, Department of Mechanical Engineering, Shahid Rajaee Teacher Training University, Tehran, Iran
[4] Associate Professor Department of Mechanical Engineering, Shahid Rajaee Teacher Training University, Tehran, Iran
[5] Assistant Professor, Department of Mechanical Engineering, Petroleum University of Technology, Abadan, Iran
[6] Professor, Department of Mechanical and Industrial Engineering, Norwegian University of Science and Technology, Trondheim, Norway

Highlights

- The mechanism of HIC is studied in a finger type slug catcher using advanced ultrasonic techniques and microstructural investigation methods.
- The inclusions such as elongated manganese sulfide and spherical aluminum oxide, the pearlite grains, or the interfaces of the ferrite–pearlite phases play an essential role in the HIC phenomenon as nucleation and propagation places of cracks.
- HIC cracks mostly initiate and propagate through the center of a cross-section of specimens. This region is a segregated zone where center segregation of the elements occurs.
- A linear correlation between HIC susceptibility and hardness value is recognized in steel, where by moving from distances away from the cracks (1800 µm) to the crack edge, the hardness value increases significantly (179–203 HV), confirming the diffusion of hydrogen into hydrogen traps.

Received: December 02, 2019; *revised*: January 01, 2020; *accepted*: January 25, 2020

Abstract

Although the hydrogen induced cracking (HIC) is recognized as one of the destructive modes for pipeline and component steels serving in sour environments, the behavior of the HIC is still not fully understood. On the other hand, although many efforts have been made to identify the effects of hydrogen on laboratory steel specimens, the study of actual industrial samples has received less attention. In this paper, we have studied the mechanism of the HIC in a damaged pipe of a real case study of the oil and gas industry (finger type slug catcher) using detection, characterization, and microstructural investigation methods. The detection of the HIC in the specimens by advanced ultrasonic techniques, failure analysis using tensile tests, chemical composition analysis, optical microscopy (OM), field emission scanning electron microscopy (FE-SEM), and energy-dispersive spectroscopy (EDS) techniques and their correlation with the microstructure, type, and morphology of the inclusions were conducted. The results indicated that the value of elements, especially carbon (0.13 wt %) and manganese (1.44 wt %), satisfies the requirement of API 5L specification. Furthermore, the inclusions, such as elongated manganese sulfide and spherical aluminum oxide, and the pearlite grains or the interfaces of the ferrite–pearlite phases played an essential role in the HIC phenomenon as nucleation and propagation places of cracks. It was also observed that HIC cracks were mostly initiated and propagated through the center or near the center of a

* Corresponding Author:
Email: ali_pourkamali@sru.ac.ir

cross-section of specimens. This region was a segregated zone where the center segregation of elements has occurred. Finally, we recognized a linear correlation between the HIC susceptibility and hardness value in steel, where by moving away from the cracks (1800 µm) to the crack edges, the hardness value increased significantly (179–203 HV), confirming the diffusion of hydrogen into hydrogen traps.

Keywords: Energy Dispersive Spectroscopy, Finger Type Slug Catcher, Field Emission Scanning Electron, Microscopy Hydrogen Induced Cracking

How to cite this article
Asadipoor M, Pourkamali Anaraki A, Kadkhodapour J, Sharifi M H, Barnoush A, Investigation into Mechanism of Hydrogen Induced Cracking Failure in Carbon Steel: A Case Study of Oil and Gas Industry. Iran J. Oil Gas Sci. Technol., Vol. 9, No. 3, p. 44–60, 2020.
DOI: 10.22050/ijogst.2020.210113.1529

1. Introduction

In recent years, the ever-increasing demand for oil and gas has made it important to operate safely without stopping equipment related to this industry. Steel pipes and pressure vessels are among the most important equipment in this regard. When the equipment is used in a sour environment, it poses more potential hazards to them. The most prominent threats to the structural integrity of the pipeline and equipment in acidic environments are stress corrosion cracking (SCC) and hydrogen-induced cracking (HIC). Stress corrosion cracking is a failure mode in which cracks are initiated and propagate in a corrosive environment in the presence of stresses. In the last decade, extensive studies have been conducted on this phenomenon (Raude et al., 2018; Esteban et al., 2019; Yu et al., 2020; Roccisano et al., 2020).

However, various aspects of the failure mechanism of the HIC have not been fully understood, and more extensive studies are needed in this context. In the hydrogen induced cracking phenomenon, hydrogen atoms are produced by corrosive reactions between the fluid containing moist hydrogen sulfide and the surface of steel or other sources and penetrate into the crystalline structure of steel. These atoms are usually trapped in various microsurgical imperfections such as metallurgical defects, nonmetallic inclusions, and precipitates. Hydrogen atoms in these traps combine to form hydrogen molecules. Hydrogen molecules are much larger than their atoms and cannot be released from the crystalline metal structure. With the continuation of corrosion reactions, the amount of hydrogen accumulated in discontinuities increases. When a critical amount of hydrogen is gathered in such defects, HIC cracks are initiated and propagate. Hydrogen induced cracks in the metal may be formed in the shape of an isolated HIC or clustered HIC. In the case of continuous penetration of hydrogen, the mechanical and metallurgical properties of the material are changed. When the material toughness is significantly reduced by increasing the amount of the penetrating hydrogen, stepwise cracking (SWC) is created in the vicinity of the hydrogen blisters. Propagation of these cracks toward welds or any possible discontinuity is highly dangerous and can lead to the sudden failure of the equipment (Aviles et al., 2017; Ghosh et al., 2018; Schneider et al., 2019; Mahajan et al., 2019; Asadipoor et al., 2020; Bai et al., 2020). In addition to the pipelines, the HIC phenomena can be created in a wide range of other equipment of oil and gas industry, causing considerable damage. Equipment such as pressure vessels of water absorber systems in gas pressure boost stations, glycol contact towers, glycol flash drums, glycol reboilers, finger type sludge catchers, and other equipment in contact with sour environments are other items at risk of the HIC. In storage tanks and low-pressure vessels, the damage will mostly include financial losses due to equipment degradation and environmental pollution caused by fluid leakage. However, in pressure vessels with high operational pressure, in addition to the above risks, there will be a danger of explosion and human casualties (Ghosh et al., 2018; Asadipoor et al., 2020).

Although the HIC in steel pipelines and components causes a huge amount of economic loss for the industry, the failure mechanism of the HIC is still not fully understood. On the other hand, although many efforts have been made to identify the effects of hydrogen on laboratory steel specimens, the study of actual industrial samples has received less attention. Therefore, to overcome these challenges, in this work, we have investigated the fracture mechanism of the HIC in a damaged pipe of a real case study of the oil and gas industry (finger type slug catcher) using detection, characterization, and microstructural investigation methods. The correlation of the HIC fracture mechanism with the microstructure, type, and morphology of inclusions is emphasized.

Finger type slug catcher consists of several long pieces of pipe, also known as “fingers”. These fingers are comprised of steel pipes with a diameter of 1066.8 mm (42 inches) and a length of 220 meters, working at a constant operating pressure of 4 MPa (40 bar) and a temperature of 40 °C. Indeed, during the process, fingers together constitute the buffer volume to separate the massive slugs expected from the upstream system. Figure 1(a) shows different parts of this unit. The study of process conditions and the analysis of the fluid entering the slug catcher (Table 1) indicate that by extracting and considering the main parameters, including the hydrogen sulfide gas partial pressure (40 kPa) and the pH of the aqueous (pH = 4), by ensuring the presence of free water in the system, and by conforming to the requirements of standard API 571, the occurrence or appearance of hydrogen damage in the slug catcher was probable.

Table 1

Process conditions and fluid analysis of slug catcher.

Parameter	Quantity
H_2S	0.98 mol%
CO_2	2.3 mol%
Gas temperature	40 °C
Gas pressure	40 bar
Water	0.4 mol%

a) b)

Figure 1

a) A photograph of part of the finger type slug catcher and b) removed samples from the sludge catcher.

Therefore, in the first part of this study, advanced ultrasonic techniques, including phased array (PA) and time of flight diffraction (TOFD) were used to provide the accurate detection and characterization

of defects in the body of the slug catcher. The HIC is a challenging type of defect from the ultrasonic point of view mainly due to its geometrical configuration that includes a planar component, favorable to zero degree longitudinal waves detection, and a crack-wise through-thickness component requiring an inspection with angled waves. Phased array (PA) represents a sensible step forward compared to traditional ultrasonic techniques for this application since it allows using multiple methods and angles in the same scan while registering the inspection.

In another part of this study, the effect of the microstructure and inclusions of the specimen on the hydrogen-induced cracking phenomenon was investigated. To this end, it was necessary to extract specimens from the critical locations of the component to be detected by nondestructive testing(NDT). The main objectives of this section were to investigate the crack nucleation and propagation sites of the HIC and to evaluate the distribution of the microstructural phases in the crack growth path. For these purposes, optical microscopy (OM), field emission scanning electron microscopy (FE-SEM), and energy-dispersive spectroscopy (EDS) techniques were employed to characterize the specimens. By using these methods, HIC cracks at the cross-section of the tested samples were observed, and the types of microstructural phases in the cracking region were identified. Furthermore, other aspects of the HIC such as the chemical composition analyses of microstructure and type of inclusions were performed.

2. Experimental procedures

2.1. Determining material properties and pipe grade

To identify the mechanical properties of the material and pipe grade, chemical composition analysis and tensile tests were conducted on the specimens. These samples were extracted from the pipe of the slug catcher. The chemical composition analysis was conducted using PMI Master Smart device by the emission spectrometry method using reference standard ASTM E415-15. Furthermore, the tensile test was performed with a servo hydraulic apparatus of Gotech Company in accordance with reference standard ASTM A370 (2016). It is worth mentioning that the prototype of this test was a flat section (12.63 mm × 11.00 mm), and the test was conducted at 25 °C.

2.2. Ultrasonic inspection of slug catcher subject to HIC

a. First steps in phased array application in detecting HIC defects

According to the defect nature and the last NDT results (TOFD and PA) shown in Figure 1(b), some of the most defective areas of welds and base metal of the slug catcher component containing critical defects were extracted and prepared for further nondestructive and destructive testing. Owing to the nature of the HIC defects, a planar shape and orientation in a plane parallel to the major axis of the base metal and a linear zero-degree phased array strategy were selected for flaw detection (Figure 2). Table 2 presents the equipment and test parameters.

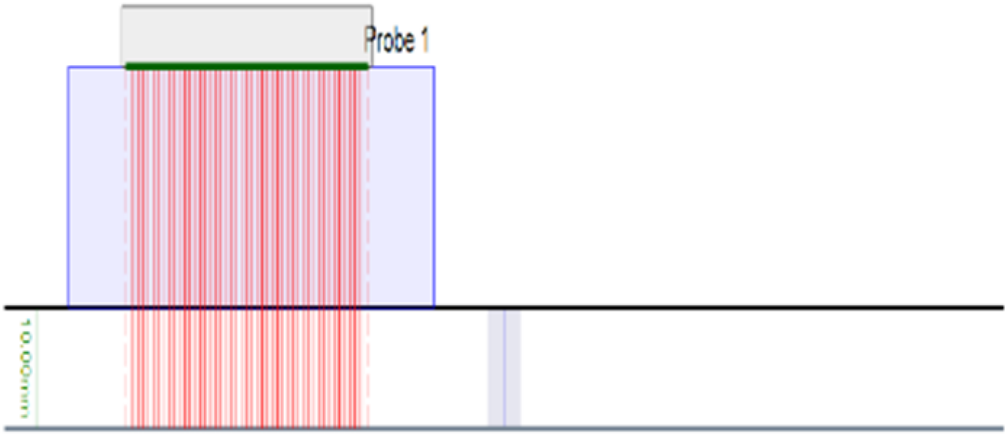

Figure 2

Scan plan of the linear zero-degree scan.

Table 2

Equipment and test parameters used for phased array flaw detection.

Subject	Description
Phased array flaw detector	Olympus Omni scan
Phased array probe	5L64-A12
Probe frequency	5 MHz
Number of probe elements	64
Phased array wedge	SA12-0L (zero degree)
Encoder	Mini wheel manual
Couplant	Glycerin
Test surface condition	Wire brush

b. Calibration and demonstration procedure

The test procedure was developed according to standard ASTM SA 578. Therefore, all of the calibration and sensitivity settings followed this standard. The reference reflector for the sensitivity setting is a back-wall signal adjusted to 75% of the full-screen height. The range of the signal was changed so that the second and third signal of the back-wall can be seen on the screen. The time corrected gain (TCG) was also calibrated in the range of zero to the third skip distance. For the designed strategy, a block was manufactured to demonstrate the ability to detect and size the accuracy of the defects. For this purpose, multiple flat bottom holes (FBH) with different diameters and depths were precisely inserted in a block with the same range of thickness and similar material (Figure 3).

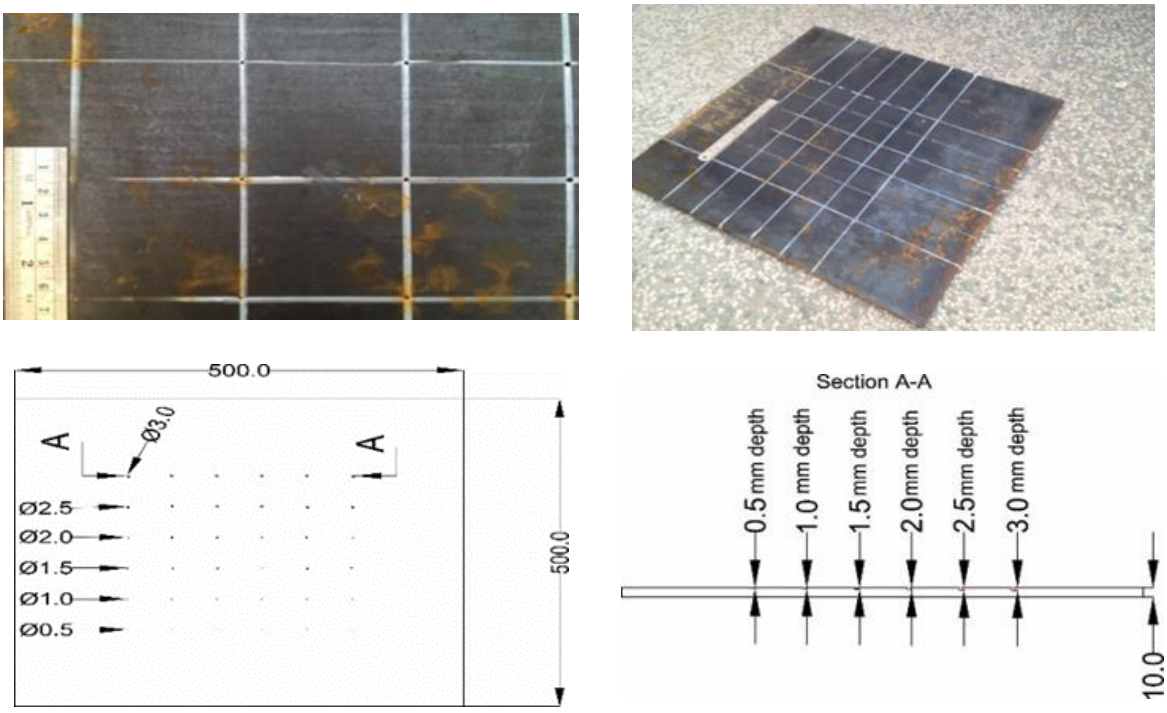

Figure 3

A schematic of a calibration block containing flat bottom holes designed for linear E-scan.

The diameter of the flat bottom holes (FBH) ranges from 0.5 to 3 mm with increments of 0.5 mm. For all sizes, it also had six holes with a depth ranging from 0.5 to 3 mm inserted at a distance of 0.5 mm. Therefore, there are 36 FBHs divided in six sizes, where each size includes six different depths (Table 3).

Table 3

Inserted flat bottom holes.

	Flat bottom hole depth (mm)					
	0.5	**1.0**	**1.5**	**2.0**	**2.5**	**3.0**
Flat bottom hole diameter (mm)	0.5	0.5	0.5	0.5	0.5	0.5
	1.0	1.0	1.0	1.0	1.0	1.0
	1.5	1.5	1.5	1.5	1.5	1.5
	2.0	2.0	2.0	2.0	2.0	2.0
	2.5	2.5	2.5	2.5	2.5	2.5
	3.0	3.0	3.0	3.0	3.0	3.0

2.3. Metallography

Metallography process was performed on the polished and etched surfaces of the extracted specimens by means of Optika-B383 MET and Olympus BX43 optical microscopes and a Quanta FEG 650 scanning electron microscope (SEM) along with Bruker flat quad 5060F energy dispersive X-ray detector (EDS). The ultrafast elemental analysis, hyperspectral mapping, microstructure analysis, and characterization of possible structural defects in the near-crack regions were conducted in accordance with standards ASTM E3-11 and ASTM E883-11. First, we ground the surface of the specimen up to 4000 SiC paper, and then polished it with 6 μm, 3 μm, and 1 μm diamond paste suspensions. Moreover,

it should be noted that the specimen was etched by a 2% nital solution for an etching time of 15 seconds.

2.4. Microhardness test

A microhardness test was performed on a specimen based on standard ISO 6507-1(2005). For this purpose, the Innova Test-Nova 240 hardness testing apparatus was utilized to measure Vickers hardness on the surface of the specimen. In this test, a load of 300 gf was applied smoothly without an impact and held in place for 10 to 15 seconds.

2.5. Fractography

To evaluate the HIC failure mechanism of the specimen and the effect of microstructure, precipitates, and inclusions on the diagnosed HIC defects, a cross-sectional area containing an HIC crack was investigated using FE-SEM and EDS techniques. A FE-SEM manufactured by TE-SCAN Company, MIRA3 model, and a Quanta FEG 650 scanning electron microscope (SEM) were used for these purposes.

3. Results and discussion

3.1. Material and pipe grade

The results of the chemical composition analysis and tensile tests demonstrated that the pipeline was made of API 5L GR. X70QS steel pipe. Tables 4 and 5 list the chemical composition and mechanical properties of this steel material under actual (as received) and standard conditions respectively.

Table 4

Chemical composition of X.70QS steel (wt %) under as-received and standard conditions.

Conditions	C	Si	Mn	S	P
As-received	0.13	0.42	1.44	0.015	0.003
Standard (maximum percentage)	0.16	0.45	1.65	0.020	0.003

Table 5

Mechanical properties of the steel under as-received and standard conditions.

Conditions	Yield strength (MPa)	Ultimate tensile strength (MPa)	Elongation to failure (%)
As-received	603	576	**23**
Standard (min–max percentage)	570–760	485–635	

3.2. Detection of HIC cracks by nondestructive tests

a. Demonstration results for a linear scan

Scanning on the demonstration block approved that the flat bottom holes (FBH) with a size of 1.5 mm and greater, with a depth of over 1 mm, and a significant diameter can be detected. However, the precise measurement is not possible due to the lower sound energy of the returned signal (Figure 4 and Table 6a).

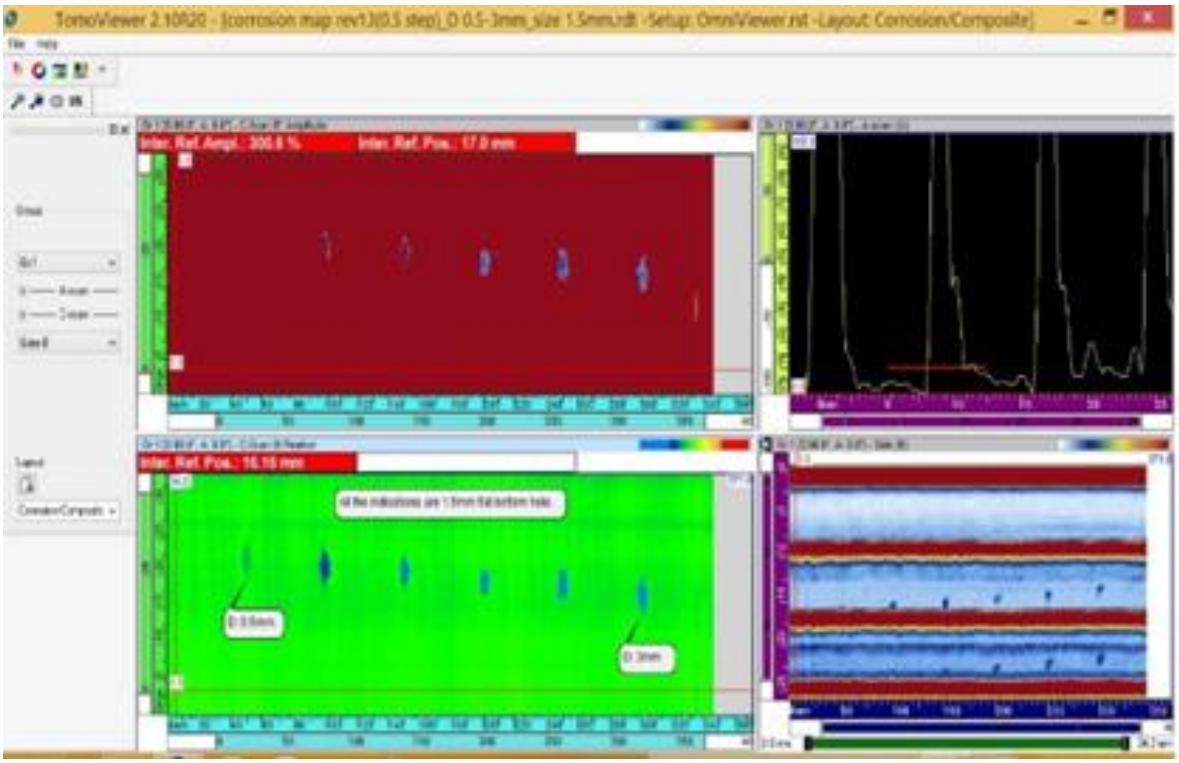

Figure 4

A schematic of the scanned data of the series of flat bottom holes with a size of 1.5 mm and a depth ranging from 0.5 to 3 mm.

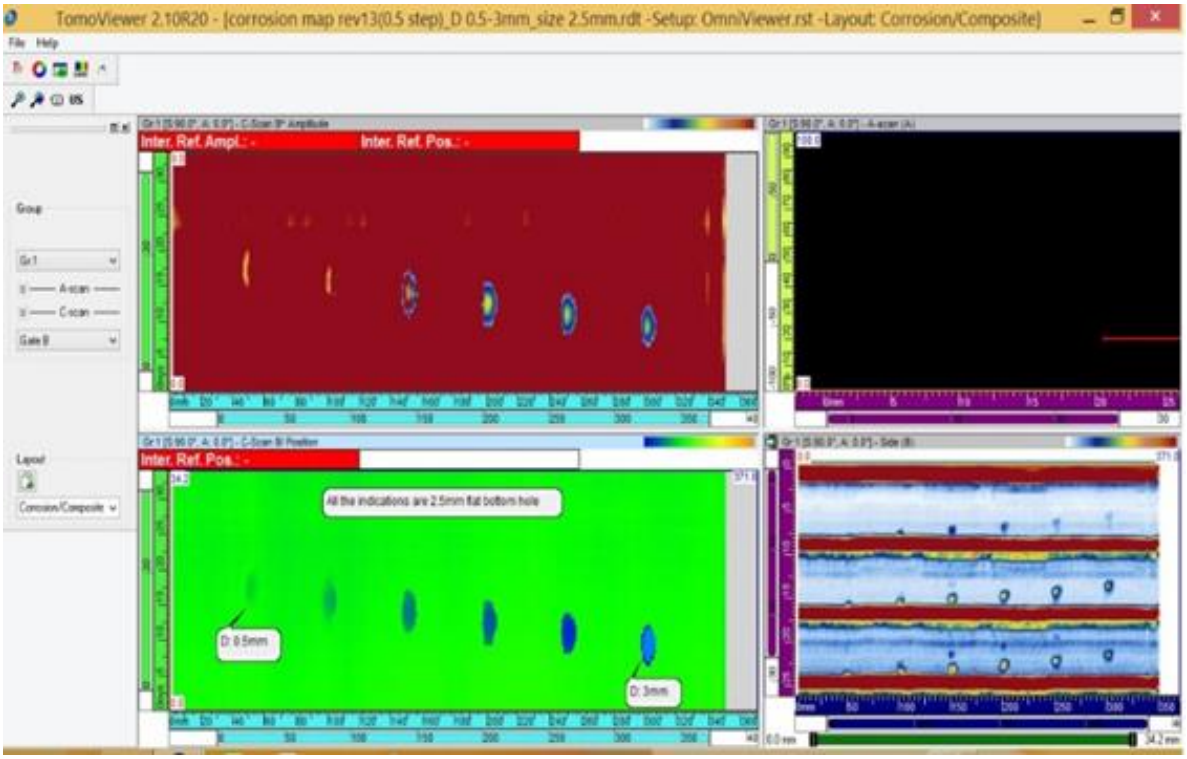

Figure 5

A schematic of the scanned data of the series of flat bottom holes with a size of 2.5mm and a depth ranging from 0.5 to 3 mm.

For the reflectors with a size of more than 2.5 mm, all the indications at a depth of 0.5 mm and higher can be detected and sized with enough signal energy and measurement accuracy (Figure 5 and Table 6b).

Table 6

(a) Detectable flat bottom hole in terms of size and depth; (b) Best measuring size and depth of FBH.

(a)	Flat bottom hole depth (mm)					
Flat bottom hole diameter (mm)	0.5	1.0	1.5	2.0	2.5	3.0
0.5						
1.0						
1.5		■	■	■	■	■
2.0		■	■	■	■	■
2.5		■	■	■	■	■
3.0		■	■	■	■	■

(b)	Flat bottom hole depth (mm)					
Flat bottom hole diameter (mm)	0.5	1.0	1.5	2.0	2.5	3.0
0.5						
1.0						
1.5						
2.0						
2.5	■	■	■	■	■	■
3.0	■	■	■	■	■	■

b. Scanning of samples and results

The samples were scanned along parallel lines drawn on the surface of test pieces (Figure 6). The distance between the lines was in such a way that enough overlap between the adjacent scans could be observed. Scanning and data collection were conducted according to the designed strategy and procedure. The typical scan parameters are listed Table 7.

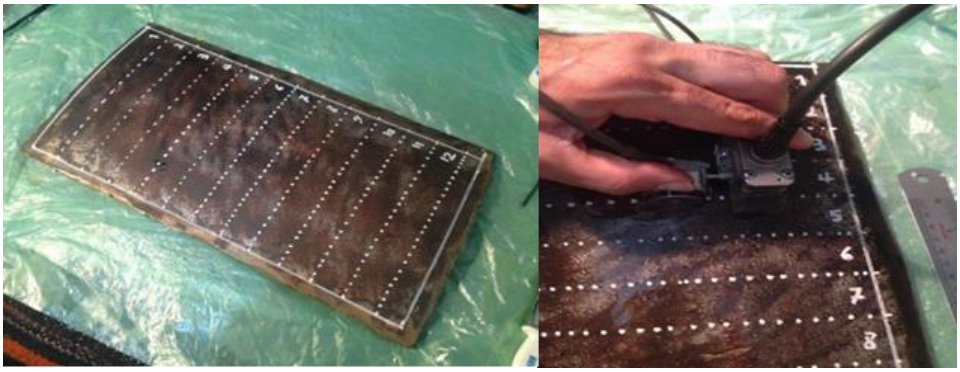

Figure 6

A schematic of the scan lines and the probe orientation along the scan lines.

Table 7

Typical focal law parameters used for scanning.

Subject	Description
Angle of incidence	0.0 degree
Wave type	Longitudinal wave
Scan Type	Manual
Min overlap between scan lines	4 mm
First element	1
Last element	64
aperture	2
Element step	1
Reference gain (dB)	24 (differ in every piece)
Scan step	1 mm

All the scanned data were interpreted in terms of detection, characterization, and sizing. The obtained data interpreted in the particular software provided with the flaw detector system. The interpretation results show that all the samples contain three typical defects, namely blisters, stepwise cracking, and inclusions, in different sizes and locations. Owing to the long service time of the component, the defects were extended through all areas of the base metal. In some cases, all the three types of defects can be seen in one line of the scan. According to the interpretation results, a sample containing sharper defects was selected for further investigations through destructive testing. During sectioning the test piece and after the macro-sectioning, the stepwise cracking and blistering are observed very clearly, and this will be a considerable improvement in all of the phased array setups and interpretations (Figures 7 and 8). Figure 7 presents the corrosion map of scan line 8 shown in Figure 6. Figures 7(a) and 7(b) illustrate the top view of the scan. Figure 7(a) is related to the height of defects or the amount of the returned energy of the reflector, while Figure 7(b) provides detailed information on the depth of a detected material flaw. According to the interpretation of the results, in the range of 0 to 40 mm, the height of ultrasonic pulse is high (orange color), and its depth is close to the center of the cross-section (green color). These symptoms represent severe damage (a blister) in the sample, as shown in Figure 7(d). Figure 8 shows a section of the blistered area after sectioning the sample in the same scanned area of Figure 7. It can be observed that the HIC cracks detected in the studied samples were mostly initiated and propagated through the center or near the center of the cross-section. This segregated zone occurred in the center of the segregation of elements, which is because the external surfaces of the slabs solidify sooner than the internal surfaces during the casting process. Therefore, the elements with a lower melting point are accumulated in the center or near the center of the cross-section.

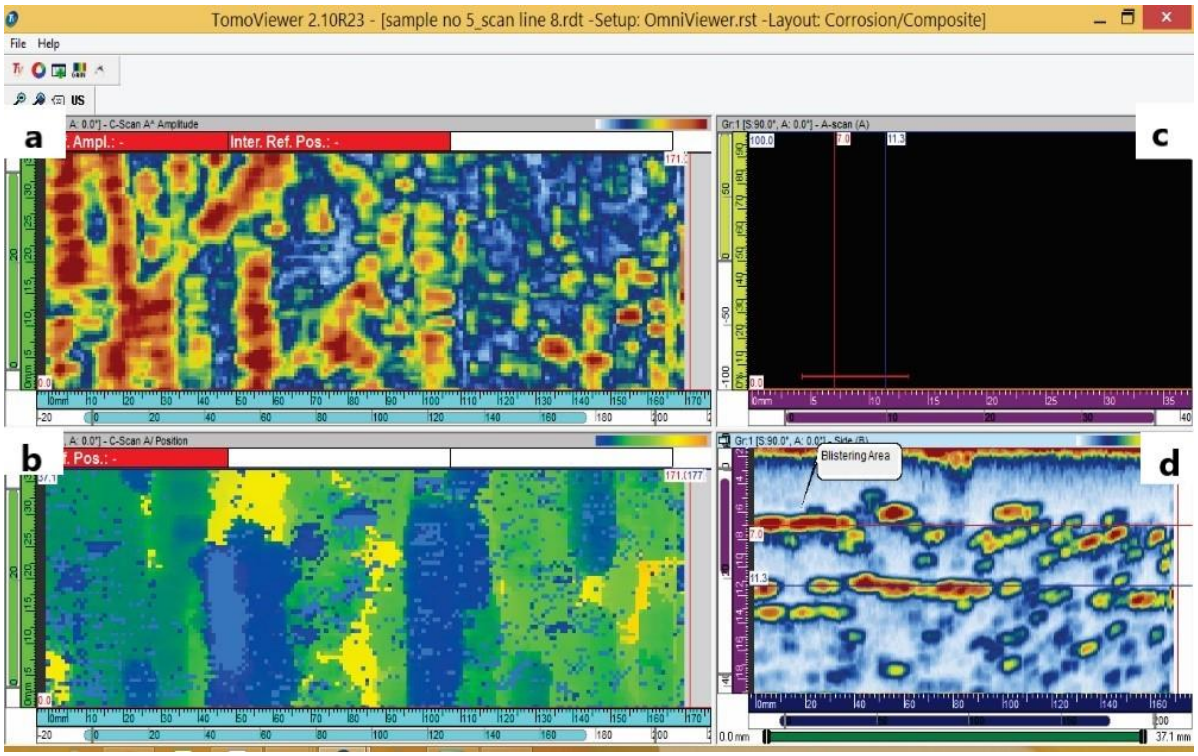

Figure 7

C-scan, B-scan, and A-scan of the phased array scanned data on the blistered area marked on the image.

Figure 8

A section of the blistered area after sectioning the sample in the same scanned area of the photo.

c. Microstructure characterization of an as-received X70QS steel

The microstructure of X70QS steel specimen was characterized by an optical microscope and a scanning electron microscope, as shown in Figure 9. The images displayed a massive ferrite microstructure with a grain size ranging from 3 to 30 μm and pearlite bands formed in the microstructure due to the steel rolling process.

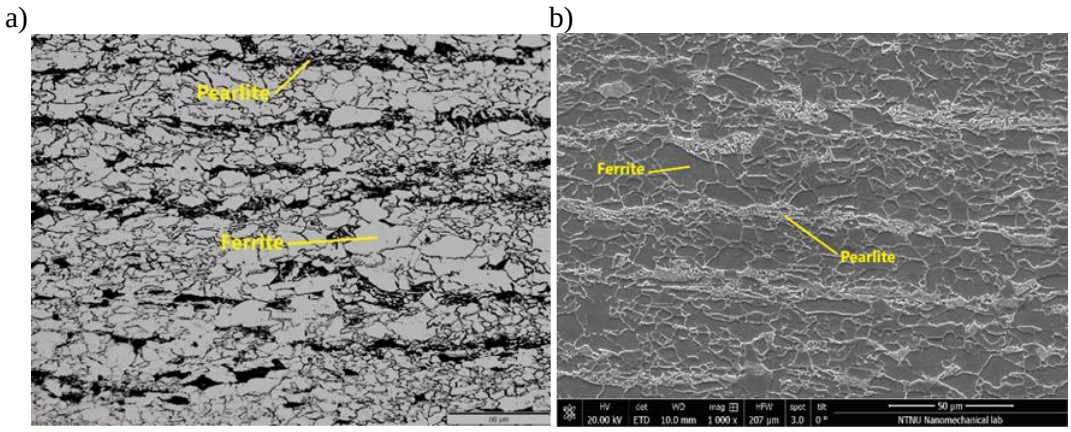

Figure 9

a) An optical microscopy image and b) a SEM image of an as-received X70QS steel specimen.

3.3. Effect of microstructure and inclusions on HIC cracks

Microstructure and inclusions are two crucial parameters influencing the nucleation and propagation of HIC cracks. Therefore, various researches have been conducted on improving the HIC resistance of pipeline and steel components to these parameters (Aviles et al., 2017; Moon et al., 2016; Venegas et al., 2014).

As mentioned earlier, the microstructure of the as-received X70QS steel specimen was composed of ferrite and pearlite phases. The ferrite is the softest phase in pipeline steel and has high resistance against the HIC. However, it is not strong enough. Accordingly, to overcome this deficiency, other elements such as carbon and manganese are added to steel, causing pearlite phase formation. Pearlite is not an independent phase and is composed of ferrite and cementite (iron carbide) phases, in which cementite

is a brittle phase increasing the strength of steel. Furthermore, as shown in Figure 9, pearlites (the dark phase) were found to be parallel to each other, and the banding phenomenon occurred in the steel structure. This defect is most likely to occur during the rolling process. Further, since the pearlite is a brittle phase, it increases the strength but reduces the fracture toughness of steel; thus, pearlite areas can be prone to nucleation and propagation of the HIC.

As displayed in Figure 10, the detected HIC in the studied specimen was formed along with the pearlite bands in the direction of the pipe axis. These pearlite bands reduced the resistance of steel to the HIC but increased its hardness by creating hydrogen trapping sites. According to Table 8, the results of the microhardness test on the specimen demonstrate that the hardness has increased in near crack regions, which confirms the diffusion of hydrogen into the hydrogen traps.

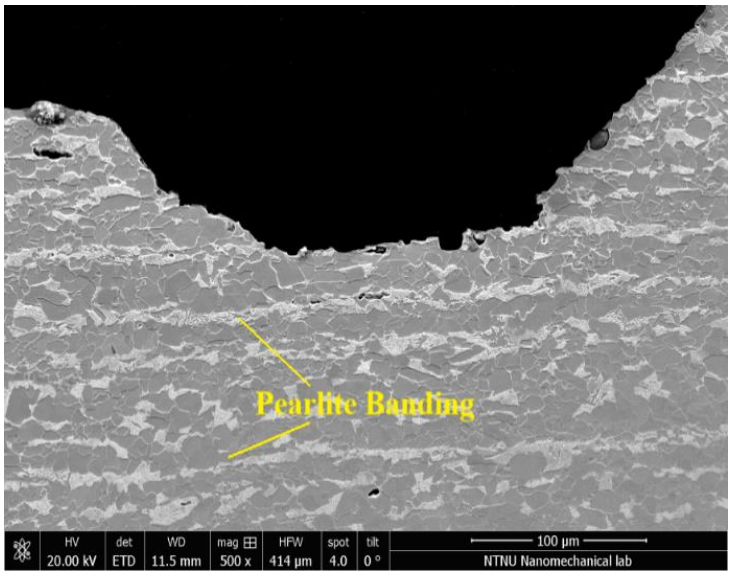

Figure 10

Banding phenomenon in the microstructure of the specimen in the direction of the pipe axis.

Table 8

Results of the microhardness of the specimen at different distances from the crack surface.

Distance from crack surface (µm)	Hardness (HV)	Maximum accepted hardness (HV)
Base Metal	179	250
1400	183	250
1000	195	250
600	196	250
200	198	250
Very close	203	250

As mentioned before, the HIC cracks detected in the studied samples were mostly initiated and propagated through the center or near the center of the cross-section (Figure 8). This segregated zone occurred in the center of the segregation of elements. It is also observed that the surface deduction of the pearlite structure in the segregated zone is higher than that in other regions, indicating that the segregated zone has higher hardness compared to other areas. As a result, this area is more sensitive to the HIC, and its microstructural investigation is highly essential.

Studies also showed that nonmetallic inclusions are recognized as the main nucleation of HIC cracks (Mohtadi-Bonab et al., 2017). Figures 11–13 reveal the presence of nonmetallic inclusions as nucleation centers of HIC cracks in the specimen. The EDS analysis in Figures 12 and 13 proved that these inclusions were elongated manganese sulfide (MnS) and spherical aluminum oxide (Al_2O_3). MnS is one of the main nucleation sites of HIC cracks. Therefore, the causes of its formation and its features are important. Manganese is added to steel to overcome the deficiency of strength and improve its hot working properties. Furthermore, the presence of manganese facilitates refining and homogenizing the weld region in X70 pipeline steel (Beidokhti et al., 2009). However, the addition of manganese to pipeline steel reduces the resistance of steel to the HIC by the formation of manganese sulfide. MnS has an elongated shape, so it provides a region with a high-stress concentration factor that can facilitate the crack initiation and propagation. Indeed, based on the hydrogen pressure theory (Zapffe et al., 1941; Tetelman et al., 1962), hydrogen atoms can diffuse into the empty region between MnS and metal matrix and combine to make hydrogen molecules, thereby leading to hydrogen pressure buildup.

a) b)

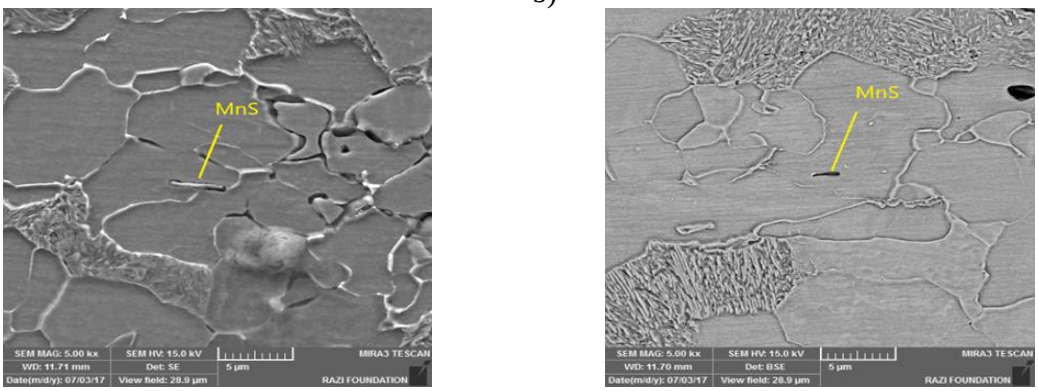

Figure 11

Presence of MnS inclusions as potential points for HIC crack initiation.

Considering the chemical composition of the as-received X70QS steel specimen (see Table 3), one can observe a high amount of manganese compared to the other elements. Therefore, the presence of elongated manganese sulfide inclusions as potential points for HIC crack initiation in the specimen is inevitable, as shown in Figures 12(a) and 12(b).

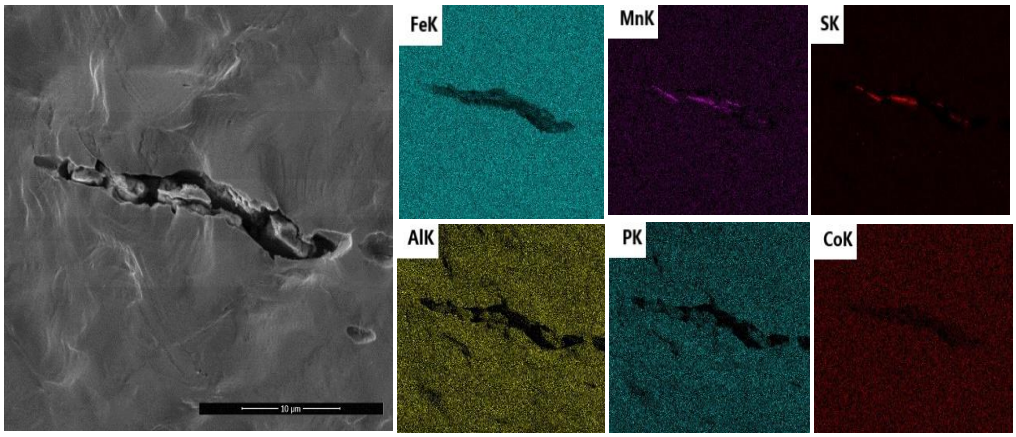

Figure 12

(a) SEM image of the HIC crack and MnS inclusions in the specimen and (b) EDS mapping images of the crack area.

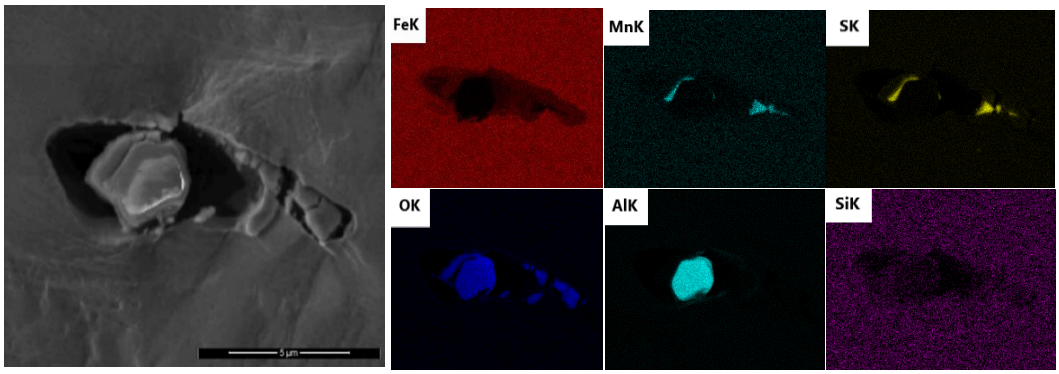

Figure 13
(a) SEM image of the HIC crack and Al_2O_3 inclusion in the specimen and (b) EDS mapping images of the crack area.

Different studies have been conducted on improving the HIC resistance of pipeline and steel components concerning these findings. For instance, in one study, Moon et al. investigated the influence of calcium addition on the HIC resistance of X70 pipeline steel (Moon et al., 2013). They found that the added calcium was combined with part of sulfur and, by forming calcium sulfide (CaS), prevented the formation of manganese sulfide. Therefore, by decreasing the amount of elongated manganese sulfide, which is recognized as the HIC crack nucleation site, the HIC susceptibility is reduced. Also, calcium sulfide inclusions have a spherical shape and cannot lead to the creation of regions with a high-stress concentration factor; accordingly, HIC cracks do not initiate from them (Moon et al., 2012; Mohtadi-Bonab et al., 2015; Hejazi, et al., 2012).

The present study showed that the HIC cracks initially nucleate in nonmetallic inclusions such as manganese sulfide and aluminum oxide, and then harder structures such as the pearlite phase provide an easy path for crack propagation. In fact, these areas provided potential sites for hydrogen trapping. As shown in Figure 14, the HIC cracks were mainly propagated in the pearlite grains or at the interfaces of the ferrite–pearlite phases. Therefore, the optimum determination of the amount of important elements such as manganese, sulfur, and aluminum in the manufacturing process is necessary to improve the mechanical properties and resistance of steel pipes and equipment to the HIC.

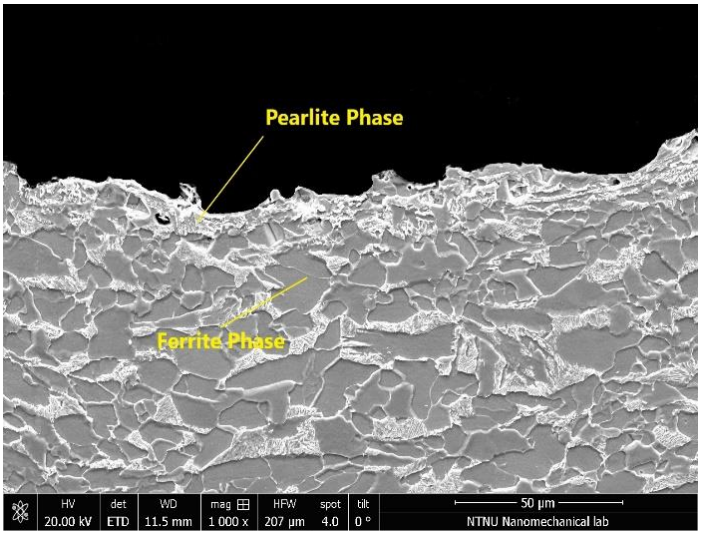

Figure 14

Propagation path of the HIC in pearlite or at the interfaces of the ferrite–pearlite phases.

4. Conclusions

Through the analysis of the as-received API 5L X70QS pipeline steel specimen by using the emission spectrometry and tensile tests and by employing optical microscopy, field emission scanning electron microscopy, and energy dispersive spectroscopy, the following findings are achieved:

- The results of PA and TOFD showed that all the samples contained three typical defects, namely blisters, stepwise cracking, and inclusions in different sizes and locations.
- The HIC cracks were mostly initiated and propagated through the center or near the center of cross-section since the surface deduction of the pearlite structure in the segregated zone was higher than that in other regions, and it had higher hardness compared to other areas.
- The optical microscopy images indicated that pearlite phases were found to be parallel to each other, and the banding phenomenon occurred in the steel structure. These pearlite bands acted as trapping sites for hydrogen atoms and produced hydrogen cracks.
- The FE-SEM images showed that the inclusions, particularly manganese sulfide or aluminum oxide, and the pearlite grains or the interfaces between the ferrite and pearlite phases—as the nucleation and propagation places of cracks—played an essential role in the HIC phenomenon.

Acknowledgments

The authors would like to express their appreciation of the support of National Iranian South Oil Company (NISOC) during this research. Also, the Norwegian University of Science and Technology (NTNU) is acknowledged for the support of this project.

Nomenclatures

EDS	Energy dispersive spectroscopy
FBH	Flat bottom holes
FE-SEM	Field emission scanning electron microscopy
HIC	Hydrogen induced cracking
OM	Optical microscopy
PA	Phased array
SCC	Stress corrosion cracking
SWC	Stepwise cracking
TCG	Time corrected gain
TOFD	Time of flight diffraction

References

Asadipoor, M., Anaraki, A. P., Kadkhodapour, J., Sharifi, S. M. H., and Barnoush, A., Macro-and Microscale Investigations of Hydrogen Embrittlement in X70 Pipeline Steel by In-situ and Ex-Situ Hydrogen Charging Tensile Tests and In-situ Electrochemical Micro-cantilever Bending Test, Materials Science and Engineering: A, Vol. 772, 138762p, 2020.

Aviles, J. Q., Alonso-Falleiros, N., and De Melo, H. G., Hydrogen Induced Cracking HIC Resistance in HSLA API 5L X65 E 5L X80 Steels, in OTC Brazil, Offshore Technology Conference, October, 2017.

Bai, P. P., Zhou, J., Luo, B. W., Zheng, S. Q., Wang, P. Y., and Tian, Y., Embrittlement of X80 Pipeline

Steel in H_2S Environment: Effect of Hydrogen Charging Time, Hydrogen-trapped State and Hydrogen Charging–releasing–recharging Cycles, International Journal of Minerals, Metallurgy and Materials, Vol. 27, No.1, p. 63–73, 2020.

Beidokhti, B., Koukabi, AH., Dolati, A., Influences of Titanium and Manganese on High Strength Low Alloy SAW Weld Metal Properties, Mater Charact, Vol. 60, p. 225–33, 2009.

Esteban, P., Calleja, B., Astigarraga, V., and López, A., Stress Corrosion Cracking of Super duplex Stainless Steels for Use in H_2S Containing Environments in Oil and Gas Production, in CORROSION 2019, NACE International, May, 2019.

Ghosh, G., Rostron, P., Garg, R., and Panday, A., Hydrogen Induced Cracking of Pipeline and Pressure Vessel Steels, A Review, Engineering Fracture Mechanics, Vol.199, p. 609–618, 2018.

Hejazi, D., Haq, AJ., Yazdipour, N., Dunne, DP., Calka, A., Barbaro, F., and Pereloma, EV., Effect of Manganese Content and Microstructure on The Susceptibility of X70 Pipeline Steel to Hydrogen Cracking, Mater Science Engineering A, Vol. 551, p. 40–49, 2012.

Mahajan, D. K., Singh, V., Arora, K. S., and Singh, R., Hydrogen Induced Blister Cracking and Mechanical Failure in X65 Pipeline Steels, 2019.

Mohtadi-Bonab, MA., Eskandari, M., A Focus on Different Factors Affecting Hydrogen Induced Cracking in Oil and Natural Gas Pipeline Steel, Engineering Failure Analysis, Vol. 79, p. 351–360, 2017.

Mohtadi-Bonab, MA., Szpunar, JA., Basu, R., and Eskandari, M., The Mechanism of Failure by Hydrogen Induced Cracking in an Acidic Environment for API 5L X70 Pipeline Steel, International Journal of Hydrogen Energy, Vol. 40, p.1096–107, 2015.

Moon, J., Choi, J., Han, S. K., Huh, S., Kim, S. J., Lee, C. H., and Lee, T. H., Influence of Precipitation Behavior on Mechanical Properties and Hydrogen Induced Cracking During Tempering of Hot-Rolled API Steel for Tubing, Materials Science and Engineering: A, Vol.652, p.120–126, 2016.

Moon, J., Kim, SJ, and Lee, C., Role of Ca Treatment in Hydrogen Induced Cracking of Hot Rolled API Pipeline Steel in Acid Sour Media, Metals and Material International, Vol. 19, p. 45–8, 2013.

Moon, J., Park, C., and Kim, SJ., Influence of Ti Addition on The Hydrogen Induced Cracking of API 5L X70 Hot-rolled Pipeline Steel in Acid Sour Media, Metals and Material International, Vol. 18, p. 613–7, 2012.

Raude, A., Bouchard, M., and Sirois, M., Stress Corrosion Cracking Direct Assessment of Carbon Steel Pipeline Using Advanced Eddy Current Array Technology, in CORROSION 2018, NACE International, 2018.

Roccisano, A., Nafisi, S., and Ghomashchi, R., Stress Corrosion Cracking Observed in Ex-Service Gas Pipelines: A Comprehensive Study, Metallurgical and Materials Transactions A, Vol.51, No.1, p.167–188, 2020.

Schneider, C., An Investigation into Hydrogen-induced Cracking and Delamination, 2019.

Tetelman, AS., and Robertson, WD., The Mechanism of Hydrogen Embrittlement Observed in Iron-silicon Single Crystals, Transactions of the American Institute of Mining, Metallurgical, and Petroleum Engineers, Vol. 224, p. 775–83, 1962.

Venegas, V., Caleyo, F., Herrera, O., Hernández-Sánchez, J., and Hallen, JM., Crystallographic Texture Helps Reduce Hydrogen Induced Cracking in Pipeline Steels, International Journal of

Electrochemical Science, Vol. 9, p. 418–25, 2014.

Yu, Z., Chen, J., Yan, H., Xia, W., Su, B., Gong, X., and Guo, H., Degradation, Stress Corrosion Cracking Behavior and Cytocompatibility of High Strain Rate Rolled Mg-Zn-Sr Alloys, Materials Letters, Vol.260, p.126920, 2020.

Zapffe, C., and Sims, CE., Hydrogen Embrittlement, Internal Stress and Defects in Steel, Transamerican INS Min Metal Engineering, Vol. 145, p. 225–32, 1941.